

UNCLASSIFIED

Copy No. 6

RM No. A8H03

CLASSIFICATION CHANGED

To UNCLASSIFIED

~~CONFIDENTIAL~~
NACA

By authority of *H. L. Dryden* Date *6-11-53*
per naca Release form #1478. By HLR, 8-5-53.

RESEARCH MEMORANDUM

SOME PRELIMINARY RESULTS IN THE DETERMINATION OF
AERODYNAMIC DERIVATIVES OF CONTROL SURFACES IN
THE TRANSONIC SPEED RANGE BY MEANS OF A
FLUSH-TYPE ELECTRICAL PRESSURE CELL

By Albert L. Erickson and Robert C. Robinson

Ames Aeronautical Laboratory
Moffett Field, Calif.

CLASSIFIED DOCUMENT

This document contains classified information affecting the National Defense of the United States within the meaning of the Espionage Act, USC 5011 and 50. Its transmission or the revelation of its contents in any manner to an unauthorized person is prohibited by law. Information so classified may be imparted only to persons in the military and naval services of the United States, appropriate civilian officers and employees of the Federal Government who have a legitimate interest therein, and to United States citizens of known loyalty and discretion who of necessity must be informed thereof.

NATIONAL ADVISORY COMMITTEE
FOR AERONAUTICS

WASHINGTON
October 8, 1948

NACA RM No. A8H03

~~CONFIDENTIAL~~

UNCLASSIFIED

UNCLASSIFIED

NATIONAL ADVISORY COMMITTEE FOR AERONAUTICS

RESEARCH MEMORANDUM

SOME PRELIMINARY RESULTS IN THE DETERMINATION OF AERODYNAMIC
DERIVATIVES OF CONTROL SURFACES IN THE TRANSONIC SPEED RANGE

BY MEANS OF A FLUSH-TYPE ELECTRICAL PRESSURE CELL

By Albert L. Erickson and Robert C. Robinson

SUMMARY

A flush-type electrical pressure cell is used for measuring rapidly changing aerodynamic forces on a fluttering control surface. By means of this method, fluctuations of pressure on an airfoil may be measured during flutter and the corresponding variations of hinge moment may be computed. Data are presented for one cycle of control motion in order to show the applicability of the technique. It is concluded that this technique is valuable for the measurement of aerodynamic forces. It is pointed out that the method has special merit in the investigation of two-dimensional effects and the study of upper and lower surfaces independent of one another.

Some interesting results obtained using the flush-type electrical pressure cells are presented. It is shown that separation has two effects: First, it reduces the hinge moment as might be expected; and, second, it increases the time lag of the hinge moment. Therefore, the upper and lower surfaces are affected in a considerably different manner. It is further shown that the nonlinear static hinge moment can be closely approximated by the fundamental resultant hinge moment plus the in-phase portion of the second harmonic.

INTRODUCTION

Generally speaking, the measurement of oscillating aerodynamic forces by the usual methods requires the precise determination of all mechanical forces and, for two-dimensional results, the complete elimination of end effects. These requirements can be dispensed with if the aerodynamic forces at midspan can be measured directly

UNCLASSIFIED

by a device such as an instantaneous recording pressure cell.

The present report deals with the application of such a pressure-measuring technique to the direct measurement of aerodynamic forces in the investigation of transonic flutter of control surfaces in the Ames 16-foot high-speed wind tunnel.

SYMBOLS

The symbols used in this report are defined as follows:

Ch_a	aileron hinge-moment coefficient $\left(\frac{H}{q b_a \bar{c}_a^2} \right)$
H	hinge moment, inch-pounds
H_0	hinge-moment vector, inch-pounds
M	free-stream Mach number
P	pressure coefficient $\left(\frac{p-p_s}{q} \right)$
ΔP	pressure-coefficient increment $\left(\frac{\Delta p}{q} \right)$
b_a	aileron span, inches
\bar{c}_a	root-mean square aileron chord, inches
f	flutter frequency, cycles per second
p	local static pressure, pounds per square inch
Δp	local static pressure change, pounds per square inch
p_s	free-stream static pressure, pounds per square inch
q	dynamic pressure, pounds per square inch
t	time, seconds
α	angle of attack, degrees
δ_a	aileron angle, degrees or radians
δ_{a_0}	aileron position vector, degrees or radians

- ϕ phase angle relative to the starting point of the analysis,
radians
- ω circular frequency ($2\pi f$), radians per second

MODEL AND INSTRUMENTATION

Model


Figure 1 shows the model mounted in the wind tunnel with some of the test instruments in the foreground. The upper half of the tunnel shell is partially opened and appears at the top of the photograph. The model was the same partial-span wing described in reference 1 except that the aileron was divided into three parts of equal span to reduce the loads which had resulted in structural failures during earlier tests. The inboard and outboard sections were restrained at zero aileron angle, while the center portion, which had a span of 28.75 inches, was used for the flutter tests. As in reference 1, the wing was restrained in bending and torsion by a tip strut. A chordwise row of 23 pressure cells and a parallel row of static-pressure orifices were installed at a station 8.75 inches from the outboard end of the portion of the aileron tested.

The Pressure Cell

The pressure cells used in this test (fig. 2) were of a special design having a pressure-sensitive diaphragm flush with the airfoil surface to avoid the phase and amplitude errors present when tubular or orifice connections are used. The diaphragm was made of 0.003-inch steel and was soldered to a 1/2-inch-diameter steel cylinder. A 120-ohm strain gage was cemented directly to the inner surface of the diaphragm and the electrical and reference pressure leads were taken out through an insulating plug at the other end of the cylinder. The natural frequency of this assembly was approximately 6000 cycles per second. In this test the free-stream static pressure was used as the reference pressure for all cells.

Electrical Instrumentation

The degree of amplification and stability required of an electrical system to operate with the flush-diaphragm pressure cells was not to be found in any commercially available equipment.



Therefore, special equipment was designed by the NACA.

An oscillator having a frequency of 2000 cycles per second was used to supply the bridge voltage for a resistance bridge, one leg of which was the pressure-cell strain gage. In operation, the bridge was unbalanced a predetermined amount and the strain-gage pickup changed the unbalance in proportion to the pressure to be measured. The modulated carrier current was then amplified and rectified and indicated pressure changes with appropriate sign. Only 15 amplifier channels were available for this test so the data for 8 cells on the aileron and 7 cells on the wing were recorded.

All data from 15 pressure cells, 4 accelerometers for indicating wing motion, a strain gage, an aileron position indicator, and a time reference were recorded by two oscillographs. The strain gage measured the force exerted by a hydraulic damper. The aileron position and the time reference were recorded by both instruments, which operated simultaneously. Correlation between the two records was made by using the time reference to match cycles, with the exact correlation coming from the aileron-position trace.

Precision

In calibrating the pressure cells, it was found that temperature changes caused a relatively large zero drift but that the slope of the calibrations was essentially unchanged. This is illustrated for one cell in figure 3. For the tests, the bridge circuit balance was adjusted so that the entire calibration fell within the linear range of the amplifier. Static calibrations of four typical cells appear in figure 4.

The frequency response of the pressure-cell-amplifier system was investigated by imposing a known pressure variation on the pressure cells at several frequencies. The dynamic response corresponded to the static calibration for frequencies up to 20 cycles per second. At 30 cycles per second the response had dropped 7.5 percent, at 40 cycles 17 percent, and at 60 cycles 33 percent. In the total hinge moment only the second harmonic is significant compared to the fundamental. The error in the second harmonic due to decreased response at 41 cycles per second (fundamental frequency 20.5 cycles per second) is about 3 percent of the fundamental. Subsequent to the test, it was found that the decreased response at the higher frequencies was due to a filter choke in the amplifier circuit. A new choke has been installed which will give, for future tests, a flat response curve up to 30 cycles per second, 1-percent loss at

50 cycles, and 2-1/2-percent loss at 100 cycles.

By using photostatic enlargements of the original oscillograph records it was possible to read time to an accuracy of 0.0003 second, or, at 20 cycles per second, 0.6 percent in frequency and phase angle, which gives a maximum possible phase-angle error of about 2.2° . The accuracy of the oscillograph timing lines was checked against a 60-cycle input and found to be better than the accuracy with which the enlarged records could be read.

Because of the zero drift mentioned above, it was possible to read only the pressure variations accurately and therefore only hinge-moment variations could be computed. However, since the control surface was floating, the hinge moment at the neutral position was zero statically and the dynamic hinge moment was the total hinge moment acting on the aileron during flutter.

To check the effect of curve fairing, one chordwise pressure variation was based on various assumed static-pressure distributions and integrated. The deviation was found to be not greater than 2-1/2 percent of the maximum hinge moment. All this deviation was due to differences in fairing the curves.

During flutter the inertia force due to acceleration of the diaphragm and strain gage produces a response which is in some cases a significant part of the total oscillogram reading. Figure 5 shows, for a frequency of 20.5 cycles per second, the computed variation of the inertia force over the chord of the aileron in terms of an equivalent pressure. Since the inertia force is 90° out of phase with velocity, the net work done by it in a complete cycle is zero. However, because the inertia force has an effect on the force component in phase with the aileron motion and on the phase angle of the resultant force, a correction was applied to the in-phase component of the total hinge moment in order to compare the aerodynamic component with the moment due to the inertia of the aileron.

RESULTS AND DISCUSSION

In order to examine the pressure-cell technique as critically as possible, the results from one cycle of motion at 20.5 cycles per second will be analyzed and checked with information or data obtained from other sources. The data for the cycle analyzed were obtained at 0.8 Mach number and 1.3° angle of attack.

General Considerations

The normal position of the aerodynamic hinge moment for static conditions as represented in a vector diagram is 180° ahead of the position vector and results in a straight-line variation of hinge moment with displacement. In the case of a self-excited oscillation, such as is discussed in this report, there is also an aerodynamic component 90° ahead of the displacement (in phase with the velocity) which produces a resultant vector leading the motion by less than 180° . A plot of the resultant hinge moment against control displacement shows a typical hysteresis loop, the area of which is a direct measure of the energy being put into the oscillating system by the aerodynamic forces. As the phase angle of the resultant hinge moment approaches that of the velocity vector (90° ahead of the displacement) the hysteresis loop becomes more open, indicating that more energy is being put into the system.

In reference 1, it was hypothesized that a time lag in the change of circulation placed the hinge-moment vector in a phase position less than 180° ahead of the control motion. The resulting hinge-moment component in phase with the velocity puts energy into the system and produces the one-degree-of-freedom oscillation known as transonic flutter.

The pressure-cell data will now be analyzed and evaluated using the concepts which have been discussed previously.

Individual Cells

The information obtained with the equipment that has been described was recorded as a function of time as shown in figure 6. The pressure data have been converted to pressure-coefficient increments and plotted in figures 7 and 8 as a function of aileron angle through one cycle of motion. The plotted points were computed for equal intervals of time. The only other basic data shown in this report are the chordwise pressures obtained with fixed aileron positions. (See figs. 9 and 10.) The instantaneous pressure data were analyzed to obtain figures 11 to 15.

Returning to figure 6, it can be seen that the aileron motion is very nearly sinusoidal, while the individual pressures are periodic at the same frequency but are not sinusoidal. The deviations from the pure wave form may be explained to some extent by the following:

(a) The sudden pressure changes through the shock would account for the square wave effect recorded by the cell at 55-percent chord on the upper surface.

(b) Some interference might be due to the wing bending at 42.3 cycles per second (aileron motion 20.5 cps), as shown by the wing-motion traces. The actual wing motion in bending was only 0.015 inch in amplitude and does not appear at lower aileron frequencies (not shown in this report), indicating that bending resonance was excited. The cell at 80-percent chord on the top surface indicates interference very nearly in phase with the wing motion. This fact coupled with the small absolute wing motion indicates a direct inertia effect on the diaphragm and not any aerodynamic two-degree-of-freedom influences.

(c) The most important causes of the nonlinearity of the final resultant are probably changes in the time lag and changes in the degree of separation through a cycle. Either one or both of these could cause the effect noted in figures 7 and 8 of opening the hysteresis loop on one part of the cycle and closing or reversing the loop direction on the other. This effect on the loop can be expressed mathematically by a second harmonic, as will be shown later.

The chordwise changes of the pressure fluctuations (figs. 11 and 12) can be explained at least to some extent by the static-pressure data (figs. 9 and 10). It is recognized, of course, that the fixed-control data do not show the effect of angular velocity or acceleration. The large pressure change at 55 percent of the chord on the top surface is caused by the passage of the shock wave over the cell with its associated large pressure change. The dynamic changes after the shock all compare with those indicated statically except that from the static data a larger variation might be expected at 80 percent of the chord. On the lower wing surface (fig. 12), two cells (49 and 57 percent) appear to be affected by the shock wave. The much larger change aft of the shock on the lower surface of the aileron as compared to the upper surface might be associated with the smaller amount of separation to be expected on the lower surface. On both surfaces, variations occur ahead of the shock which do not show up in the static plots; therefore, it is probable that these fluctuations are functions of the angular velocity and acceleration, being relatively independent of the control position. Future studies of the variations in front of the shock may be necessary.

Figures 7 and 8 are of value in that they show the time lag of the pressures relative to the aileron motion and in the case of the cells on the aileron the area within the curves is a measure of the

energy being put into or taken out of the system. From the point of view of the time lag involved, it is obvious, as mentioned before, that the time lag is changing through a cycle of motion. This effect leads to a nonlinear type of solution and, in order to determine if the system of nonlinear influences has any consistent pattern, the readings of each of the cells have been subjected to a harmonic analysis. The phase position and magnitude of the first five harmonics are shown in tables I and II. The actual aileron motion deviated from a pure wave form to the extent of containing 7.5-percent second harmonic and less than 2 percent of the third, fourth, and fifth harmonics (table III) so that the motion was of a relatively pure sinusoidal form. The reason for this purity is indicated by the phase positions of the harmonics (tables I and II) and shows up in the integrated results that will be discussed next.

Integrated Results

In order to evaluate the hinge moments, the pressures plotted in figures 11 and 12 were integrated for the first moment about the hinge line. The hinge moments for 1 inch of span due to the pressure fluctuations on the upper and lower surfaces have been evaluated independently and are shown in figures 13 and 14 as a function of aileron angle. The upper- and lower-surface components were then added vectorially to obtain the total aerodynamic hinge moment presented in figure 15. The dotted lines show the starting of the next cycle of motion which was not used in the analysis. Harmonic analysis of these results shows that of the higher harmonics only the second is significant. (See table III.) The smaller over-all harmonic content in the resultant hinge moment as compared to the individual cell pressures is caused by the different phase positions of the harmonic vectors of the individual pressures, which also indicates, as previously suggested, that variations in the time lag through a cycle cause the effective second harmonic.

Figures 16, 17, and 18 show the motion and hinge-moment variations indicated by including only the first and second harmonics of each. The test points are indicated in the figures.

It might be expected that the higher average velocity outside the boundary layer over the aft portion of the airfoil resulting from separated flow would increase the time lag, and this same separated flow would cause lower maximum hinge-moment fluctuations. Since the airfoil tested has a greater tendency toward separation on the upper surface than on the lower surface, the hinge moments obtained

from the pressure-cell data and presented in figures 13 and 14 will be examined for this effect. The maximum hinge moment acting on a 1-inch-wide chordwise strip of the upper surface is only 28 inch-pounds compared to 49 inch-pounds on the lower surface, but the upper-surface loop indicates a phase angle nearer 90° . Therefore, the energy input for the two surfaces is nearly the same, the reduced hinge moment for the upper surface being compensated by a phase angle closer to 90° .

Resolution of the Aerodynamic Moments

As explained in reference 2, periodic motions and forces may be described by the projections of rotating vectors on a line, the magnitude of the vectors being equal to the maximum displacement or force.

It is also proved in reference 2 that a harmonic force with a frequency different from that of the motion does zero net work in a time interval which includes an integral number of cycles of both force and motion. Therefore, the second and higher harmonics of the hinge moment produce zero net work during one cycle of the fundamental motion and, as the aileron motion is so nearly pure, only the fundamental hinge moments in table III will be considered in the comparison of aerodynamic and mechanical forces.

In order for a steady oscillation to exist, the resultant of the vectors which represent the varying hinge moments must be zero. If the resultant is not zero the oscillation will be either diverging or converging, depending on the vector position of the resultant. Since the amplitude of the aileron angle was relatively constant for the record from which the cycle being analyzed was taken, it is reasonable to assume that the resultant of the aerodynamic and mechanical moments should be zero and comparison will be made on this basis.

Harmonic analysis of the data in figure 15, starting at an arbitrary place in a cycle, gave the following equations for the aileron motion and the total hinge moment:

$$\delta_a = -4.65 \sin \omega t + 2.67 \cos \omega t \quad (1)$$

$$H = 45.13 \sin \omega t - 54.25 \cos \omega t \quad (2)$$

The vector diagram for these equations is shown in figure 19 where the cosine terms are plotted on the vertical axis and the sine terms on the horizontal axis. The hinge moment and aileron angle are obtained from the projections of these rotating vectors on the vertical

axis. Rotation is measured counterclockwise from the positive side of the horizontal axis. Since the inertia forces are in phase with the resultant motion and viscous damping forces lag the motion by 90° , it will be convenient to rewrite equations (1) and (2) so that the aerodynamic moment is resolved into components in phase with and 90° out of phase with the resultant of the motion vectors,

with

$$\delta_a = 5.36 \sin \omega t \quad (3)$$

then

$$H = -66.19 \sin \omega t + 24.48 \cos \omega t \quad (4)$$

A correction can now be made for the effect of the inertia of the pressure-cell diaphragms. It was found that the inertia forces of the diaphragms reduced the in-phase component by 4.88 inch-pounds, making the corrected in-phase coefficient -71.07. Figure 20 shows the vector diagram for the in- and out-of-phase components with the inertia correction included. From this diagram, it can be seen that the in-phase component of hinge moment is negative and directly opposed to the forces due to acceleration. The out-of-phase component is 90° ahead of the displacement and in phase with the velocity (negative aerodynamic damping); consequently, it puts energy into the system and must be counteracted by positive damping forces in order for a steady oscillation to exist.

Comparison of Aerodynamic With Inertia Moments

The above values of hinge moment are for a chordwise strip of 1-inch span. In order to arrive at the moments for the complete control it is necessary to assume a spanwise distribution. Since the strip being analyzed was one-third of the control span from one end of the control, it was assumed that the values obtained should be reasonable averages and they were multiplied directly by the control span of 28.75 inches to obtain one aerodynamic component of 2042 inch-pounds 180° out of phase with the motion and another of 704 inch-pounds 90° ahead of the motion and in phase with the velocity. The moment of inertia of the control surface was 1.53 inch-pounds seconds squared and the circular frequency ω of the motion was 128.9 radians per second. From these values an inertia moment of 2378 inch-pounds was computed. The viscous damping moment from the oscillograph record was 168 inch-pounds. The mechanical and aerodynamic moments for the complete

control are shown in the vector diagram of figure 21. The difference between the inertia moment and the opposing aerodynamic moment amounts to 15 percent of the inertia moment. It is believed that this is a reasonably good check on the accuracy of the pressure-cell system when the approximations involved are considered. The much larger discrepancy between the damping components is probably due to aerodynamic damping at the ends of the control.

Comparison of Static and Dynamic Hinge Moments

In reference 1, it was suggested that the static hinge moment be used as the resultant hinge moment with its position in the vector diagram being determined by the empirical phase equation presented. It is interesting to compare the dynamic results for this one cycle with what might be predicted by the method of reference 1. The resultant of the in- and out-of-phase components divided by the maximum aileron angle of 5.36° gives a hinge-moment coefficient per degree of motion of 0.016 compared with a static value of about 0.021 for the complete control. This comparison is obtained by rewriting equation (4) and including the inertia effect of the diaphragm so that

$$H = 75.2 \sin (\omega t + 2.79)$$

and then letting the phase angle (2.79 radians) equal zero which compares with the recommended procedure outlined in reference 1 for predicting the hinge-moment slope. As a further investigation, the second harmonic of the hinge moment can be written in the following manner:

$$H = 2.15 \sin 2 \omega t - 9.94 \cos 2 \omega t$$

or

$$H = 4.30 \sin \omega t \cos \omega t + 9.94 \sin^2 \omega t - 9.94 \cos^2 \omega t$$

Then in figure 22 the in-phase component is added to the resultant or

$$H = 75.2 \sin \omega t + 9.94 \sin^2 \omega t$$

These hinge moments are then plotted as a function of the aileron angle as determined from equation (1). It is interesting to note that the dynamic values tend to follow the static hinge-moment data obtained from strain-gage measurements on the complete aileron, which substantiate to a considerable degree the hypothesis of reference 1 that the dynamic resultant is not greatly different from the static hinge moments.

CONCLUDING REMARKS

A valuable technique employing electrical pressure cells has been developed for the direct measurement of oscillating air forces. Results obtained from the analysis of one cycle of motion are shown. This technique has particular advantages in the study of two-dimensional effects and also in the independent investigation of upper and lower surfaces or parts thereof.

The analysis presented in demonstrating the technique showed that an increase in separation increases the time lag and decreases the hinge moment.

It is also shown for the single case that the nonlinear static hinge moment can be approximated by the fundamental resultant hinge moment plus the in-phase portion of the second harmonic.

Ames Aeronautical Laboratory
National Advisory Committee for Aeronautics,
Moffett Field, Calif.

REFERENCES

1. Erickson, Albert L., and Stephenson, Jack D.: A Suggested Method of Analyzing for Transonic Flutter of Control Surfaces Based on Available Experimental Evidence. NACA RM No. A7F30, 1947.
2. Den Hartog, J. P.: Mechanical Vibrations. McGraw-Hill Book Co., Inc., 1940, chs. 1 and 2.

TABLE I
RESULTS OF HARMONIC ANALYSIS OF INDIVIDUAL PRESSURE FLUCTUATIONS
ON UPPER WING SURFACE

Cell location (percent chord)	Fundamental resultant pressure-coefficient increment	Magnitude of harmonics as a percent of the fundamental				Phase of a resultant for harmonics noted, ϕ (deg)				
		2	3	4	5	1	2	3	4	5
25	0.0374	52.2	14.4	5.9	8.0	286	252	248	243	270
47	.0291	47.8	14.1	6.9	3.4	131	69	14	0	0
55	.2900	8.3	16.2	7.2	4.2	358	9	355	45	42
69	.0506	41.9	8.9	8.9	2.8	288	278	207	117	135
80	.0430	27.9	18.6	8.4	16.7	278	175	0	34	326
85	.1282	20.7	6.3	3.2	2.8	274	236	263	104	124
90	.0987	18.9	7.4	3.2	3.6	304	254	106	214	236
96	.0561	46.7	7.5	3.6	1.8	274	288	135	243	270



TABLE II
RESULTS OF HARMONIC ANALYSIS OF INDIVIDUAL PRESSURE
FLUCTUATIONS ON LOWER WING SURFACE

Cell location (percent chord)	Fundamental resultant pressure-coefficient increment	Magnitude of harmonics as a percent of the fundamental				Phase of a resultant for harmonics noted, ϕ (deg)				
		2	3	4	5	1	2	3	4	5
24	0.0782	52.6	11.8	10.5	3.8	129	162	103	14	162
47	.1462	51.3	14.6	14.1	12.7	343	347	41	96	54
57	.1641	38.0	9.6	1.3	4.9	136	49	252	117	150
66	.0319	58.3	23.8	3.1	4.4	131	126	67	0	135
80	.1705	31.8	3.9	2.1	5.0	155	96	117	124	45
92	.1604	19.7	2.5	1.2	1.9	141	347	0	270	251
96	.0917	41.8	5.5	6.2	1.1	129	319	233	135	90



TABLE III
RESULTS OF HARMONIC ANALYSIS OF HINGE-MOMENT VARIATIONS
AND AILERON MOTION

Item	Fundamental resultants (in. - lb or deg)	Magnitude of harmonics as a percent of the fundamental				Phase of resultant for harmonics noted, ϕ (deg)				
		2	3	4	5	1	2	3	4	5
Upper-surface hinge moment	27.16	21.7	1.7	4.5	1.8	285	264	161	238	253
Lower-surface hinge moment	47.25	14.3	1.2	1.2	.8	324	187	3	311	242
Total hinge moment	70.57	14.4	.3	1.3	1.2	309	223	37	271	227
Aileron motion	5.36	7.5	.8	1.5	.8	150	76	143	101	93





Figure 1.- Test setup for the measuring of instantaneous pressures on a wing and control.

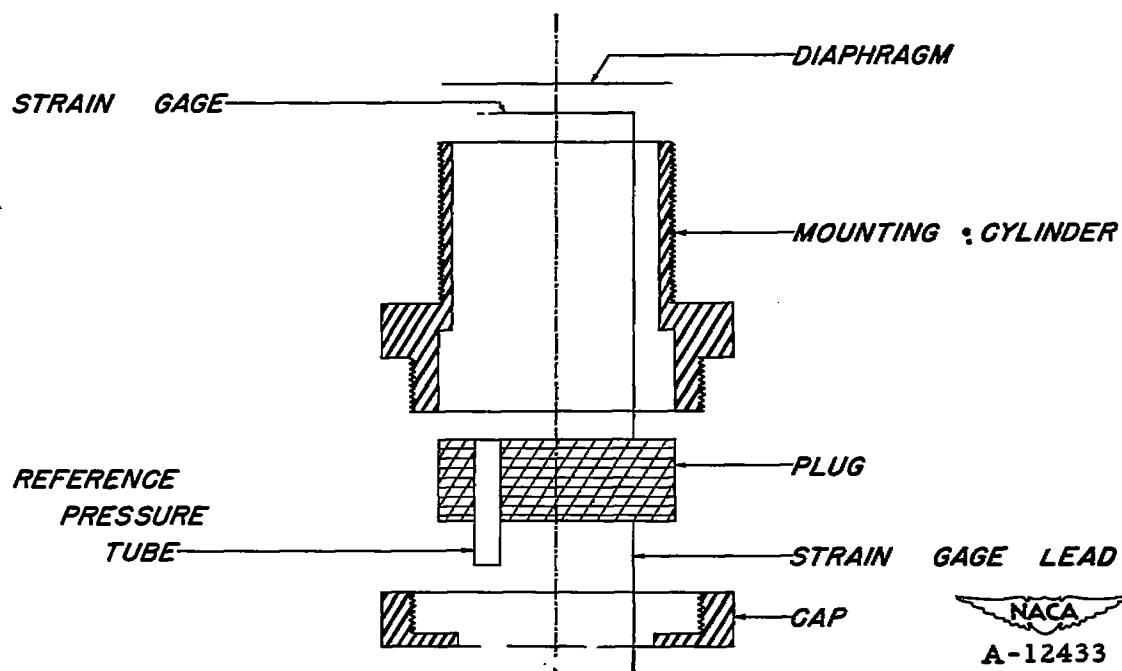
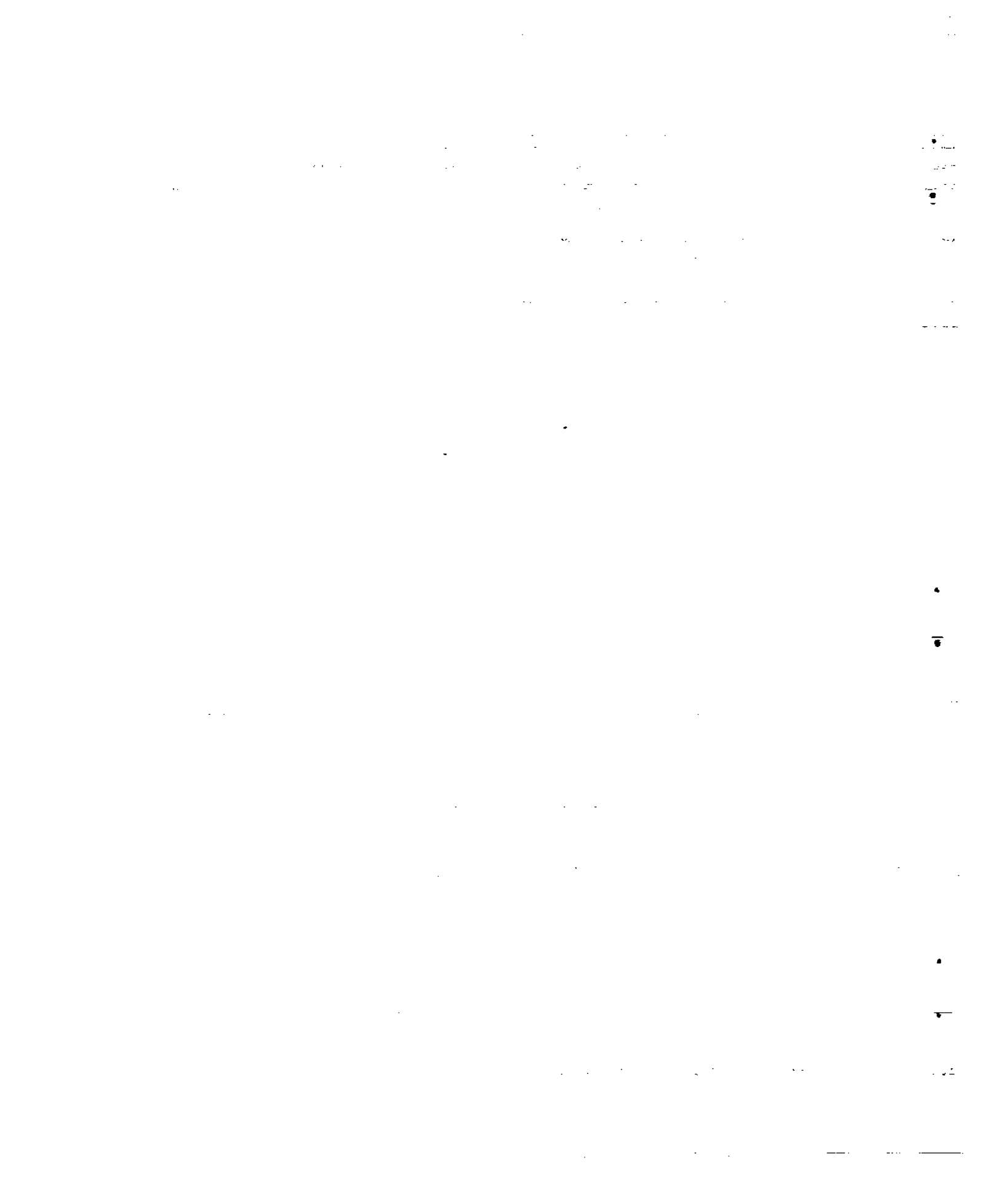


Figure 2.- Pressure cell used for measuring rapidly varying pressures.



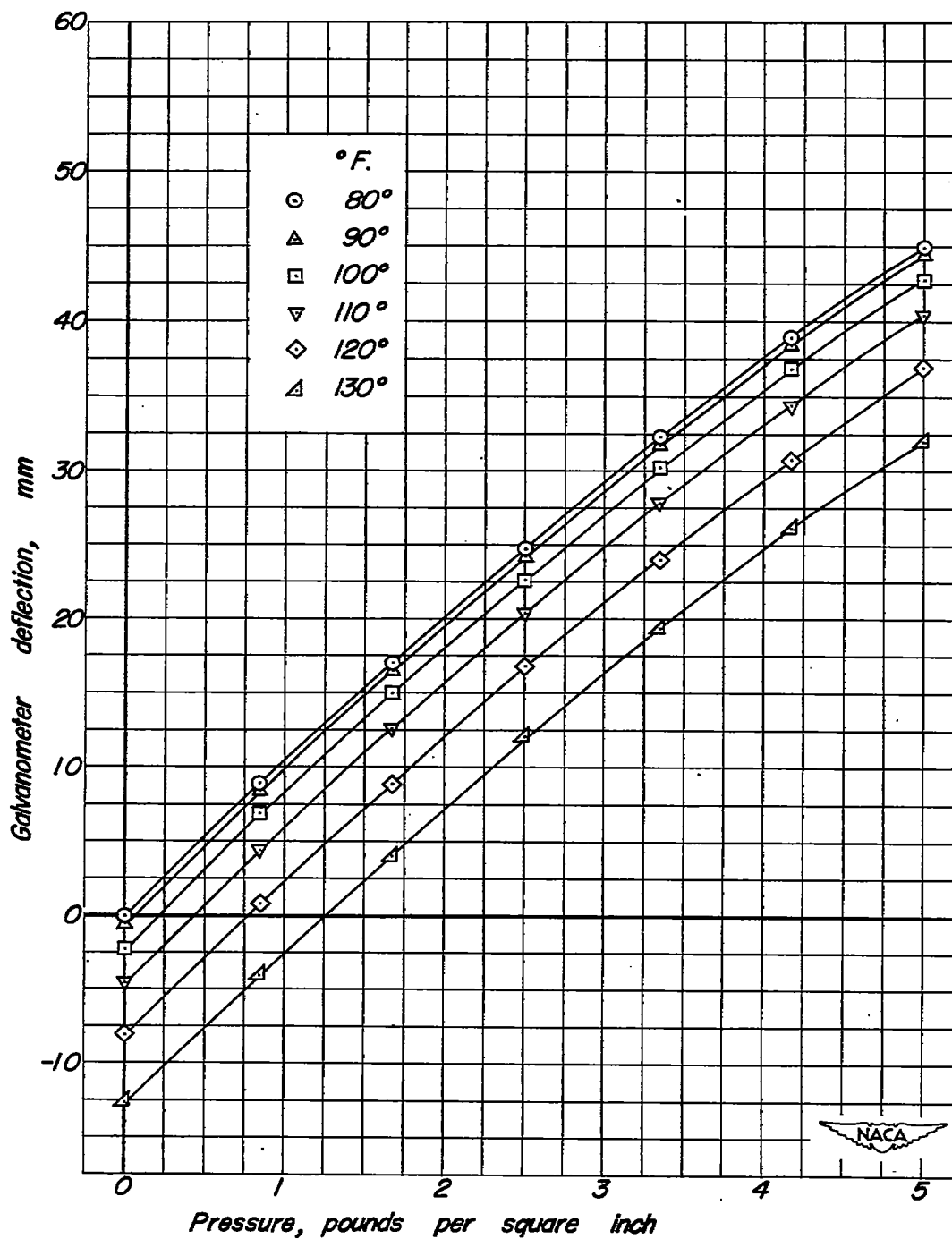


Figure 3.—Effect of temperature on dynamic pressure-cell calibrations.

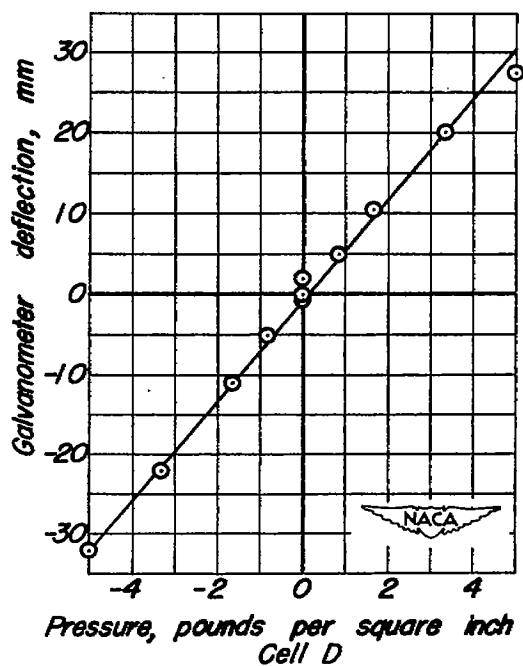
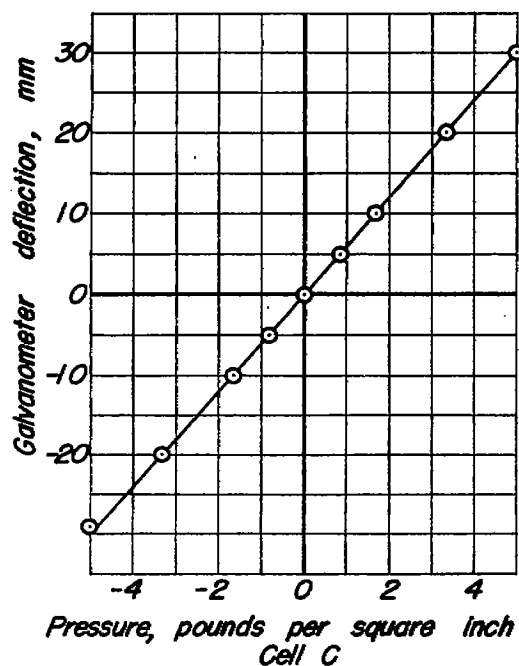
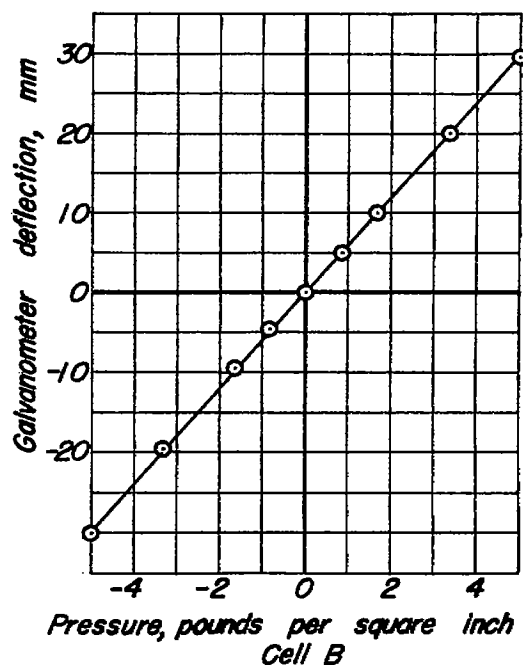
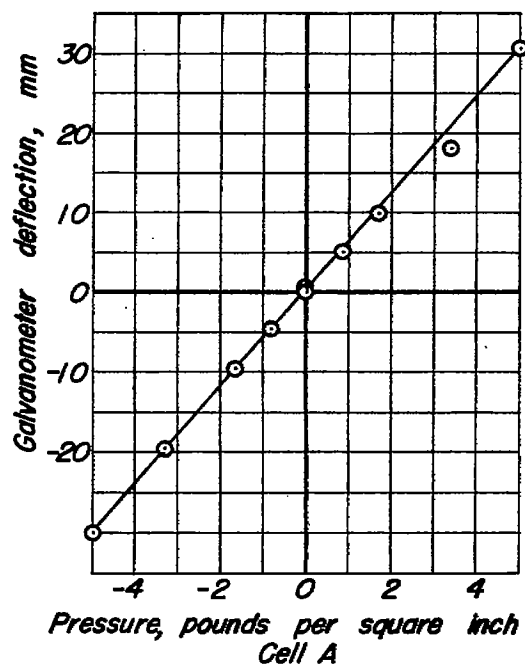


Figure 4.— Static calibrations of four pressure cells.

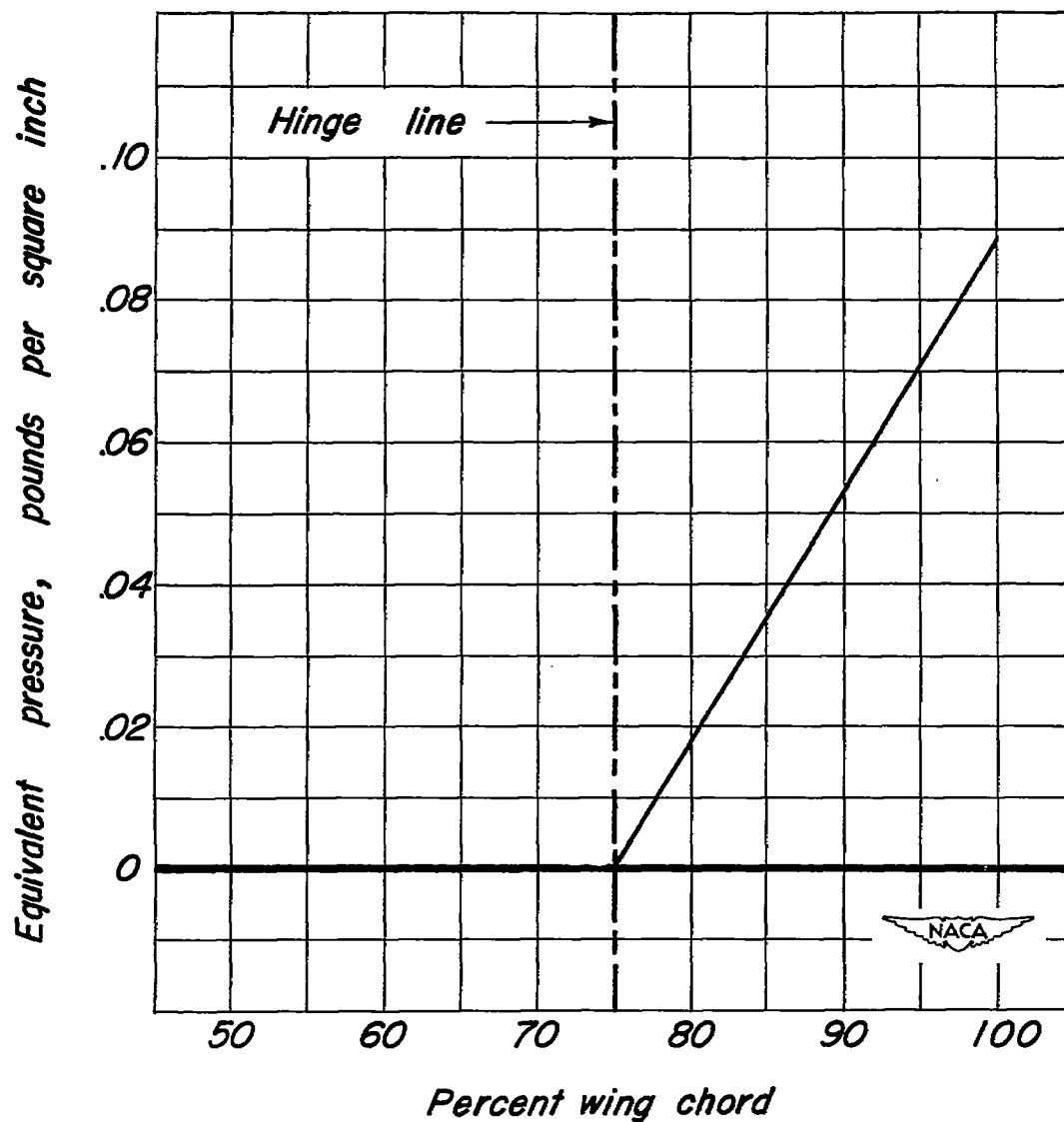


Figure 5.— Inertia force due to acceleration of the pressure-cell diaphragm and strain gage as a function of chordwise location. $f, 20.5 \text{ cps}$; $\delta_a, 5.36^\circ$

T Indicates top surface of airfoil, *B* Indicates bottom surface of airfoil.
 Number preceding letter indicates percent chord.

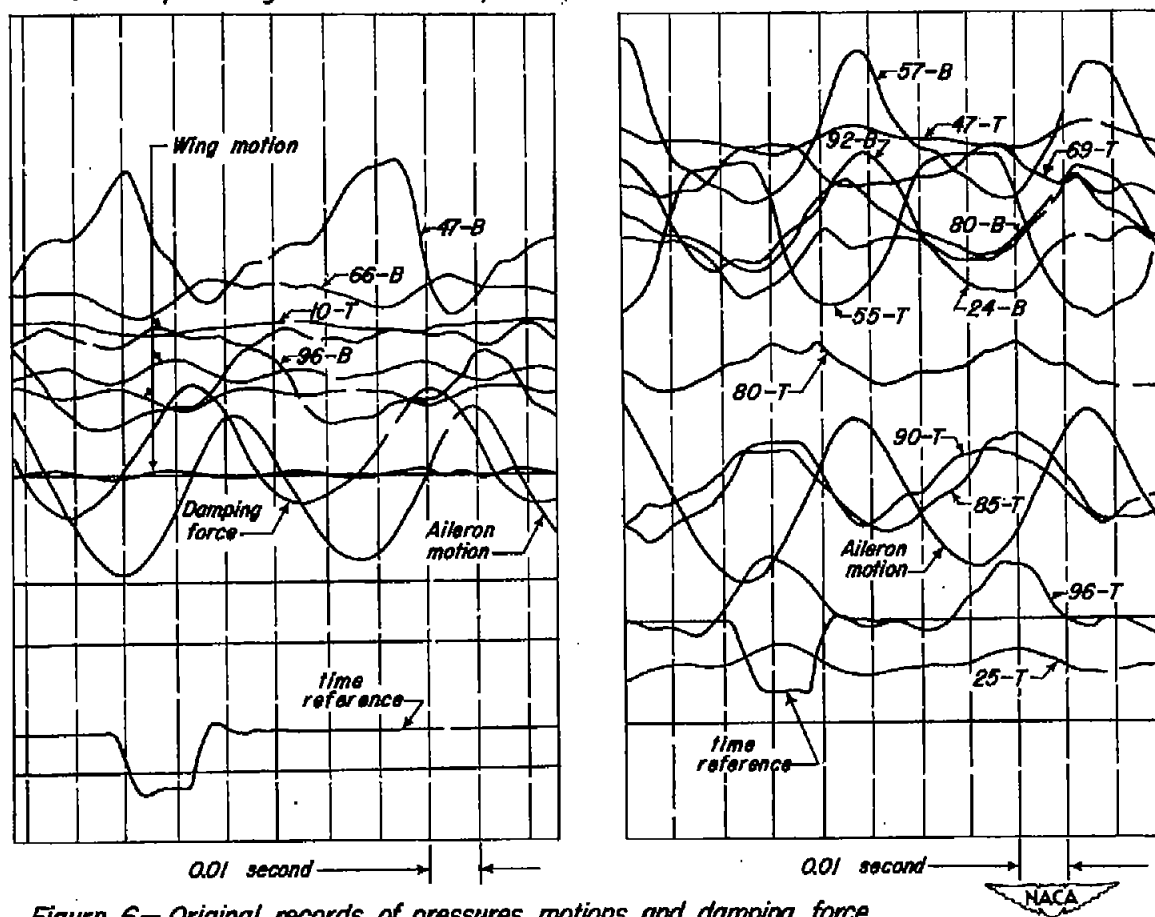


Figure 6.— Original records of pressures, motions, and damping force.

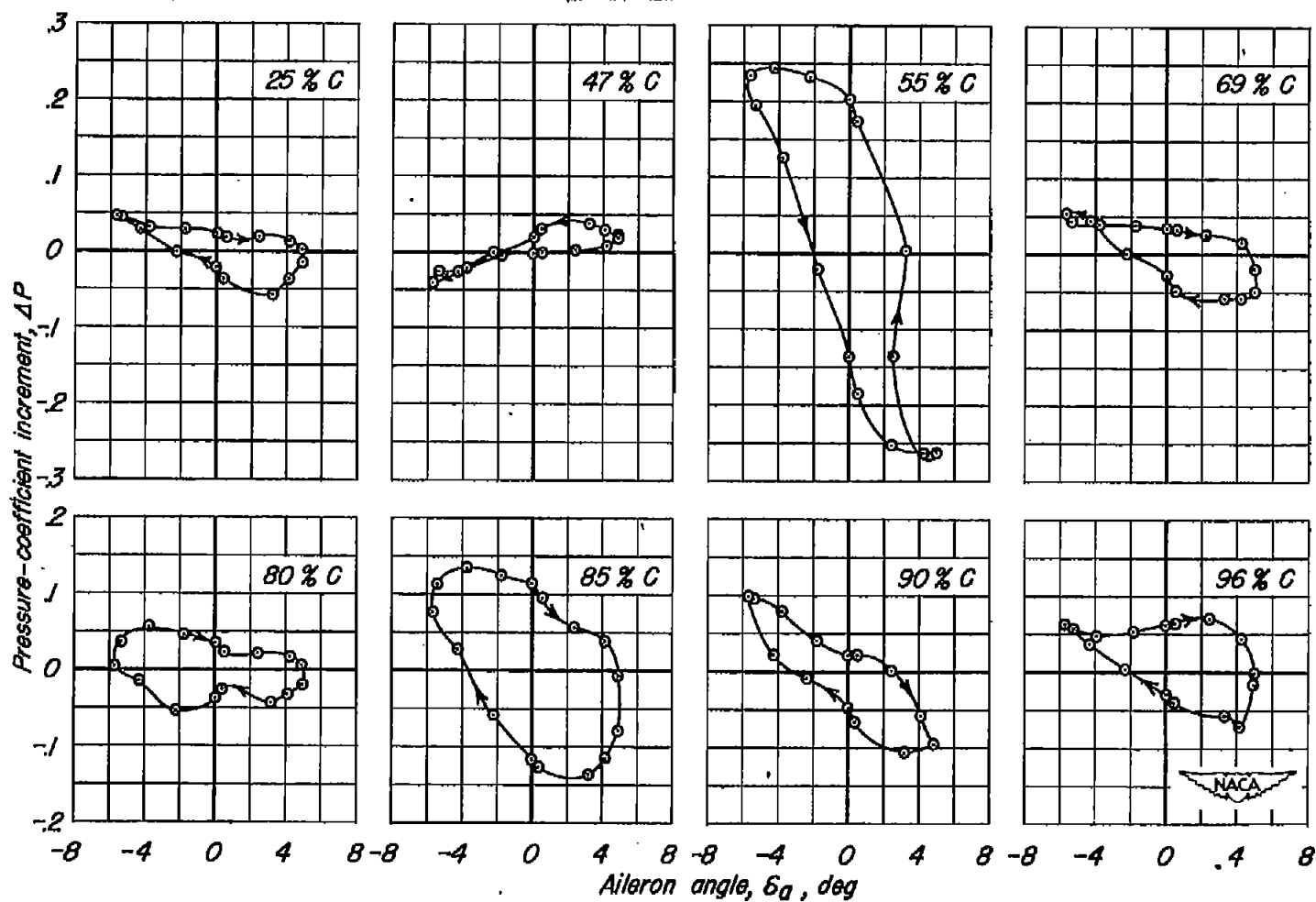


Figure 7.—Dynamic upper-surface pressures as a function of aileron angle.

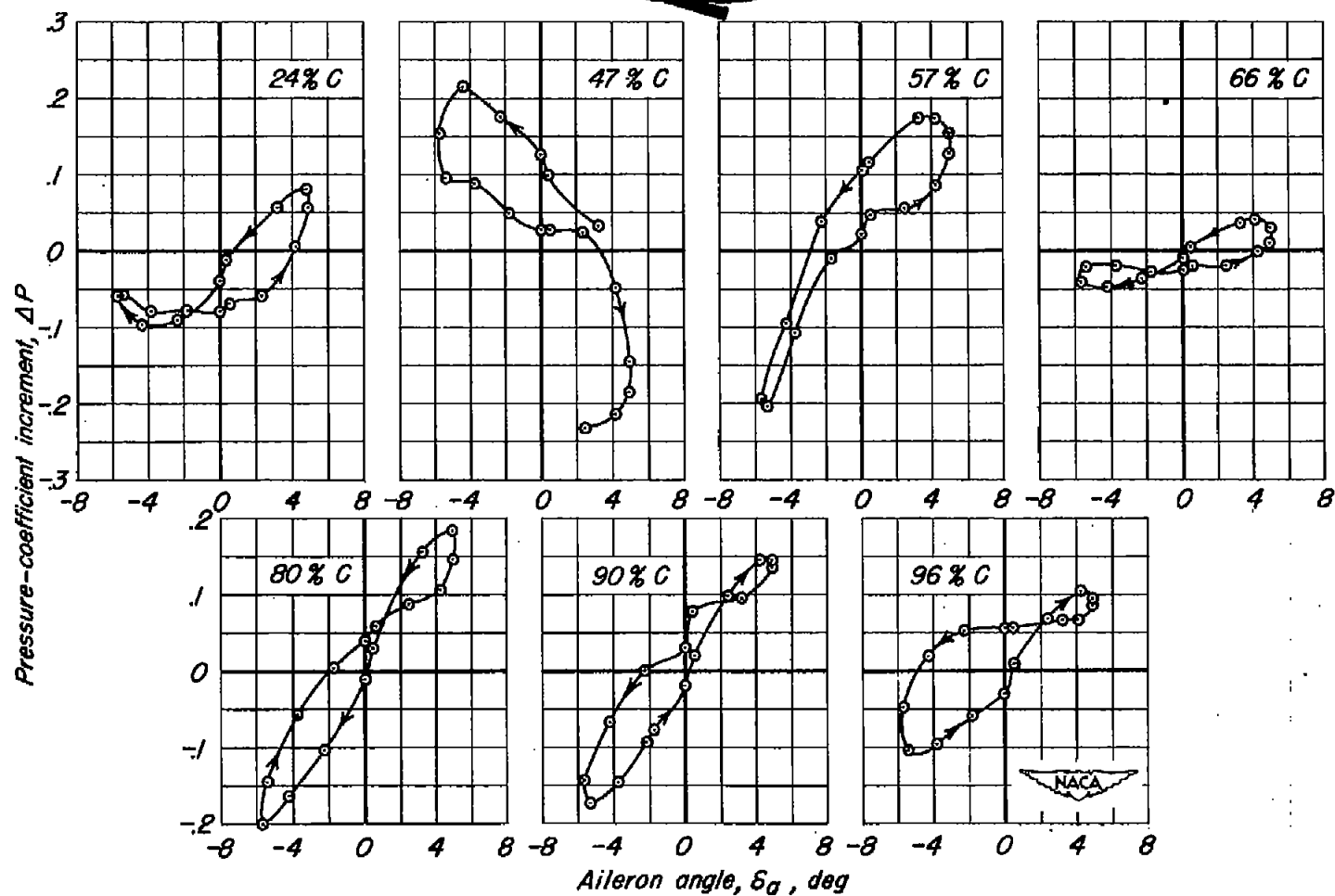


Figure 8.—Dynamic lower-surface pressures as a function of aileron angle.

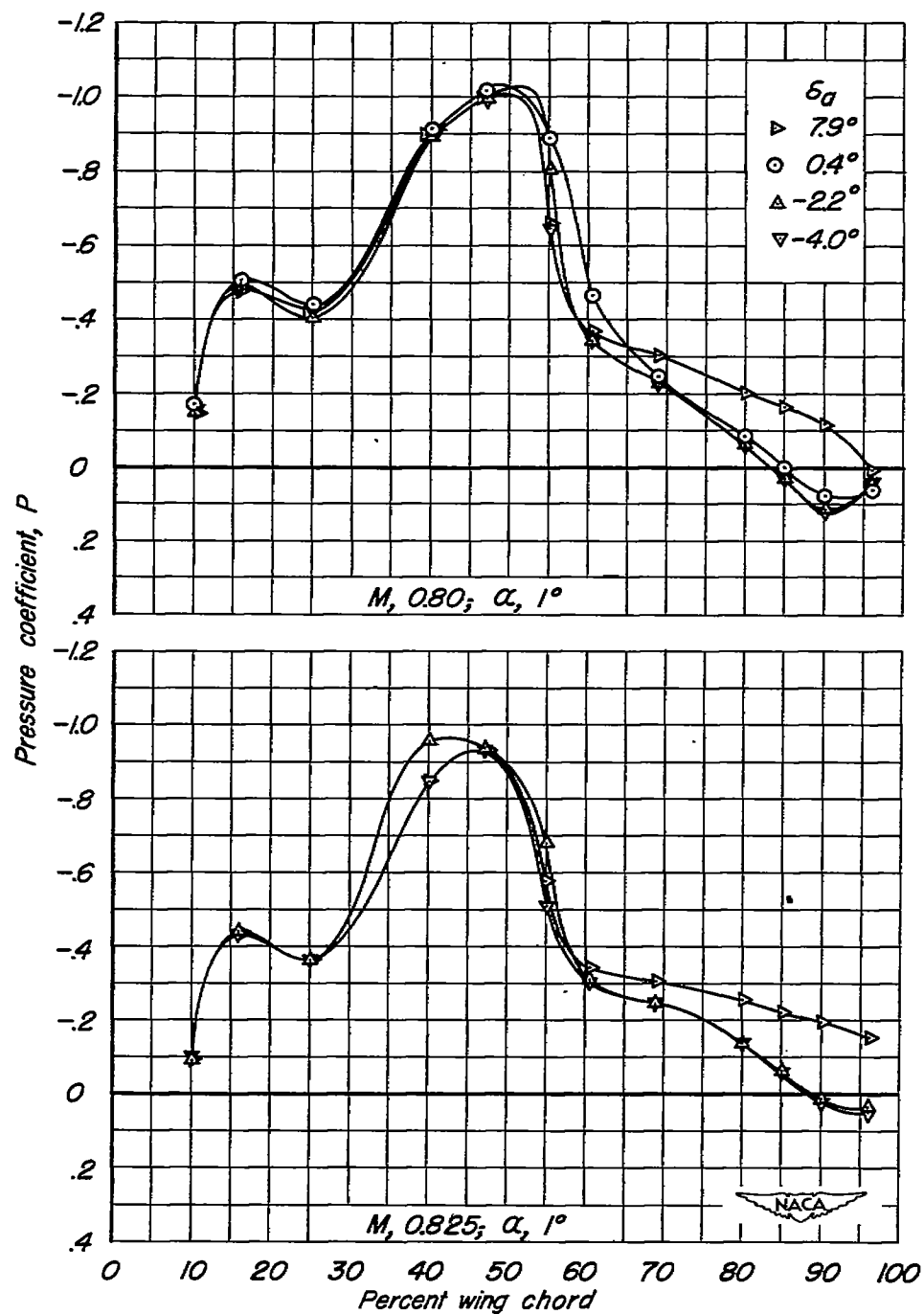


Figure 9.—Static upper-surface pressure coefficient for several aileron angles.

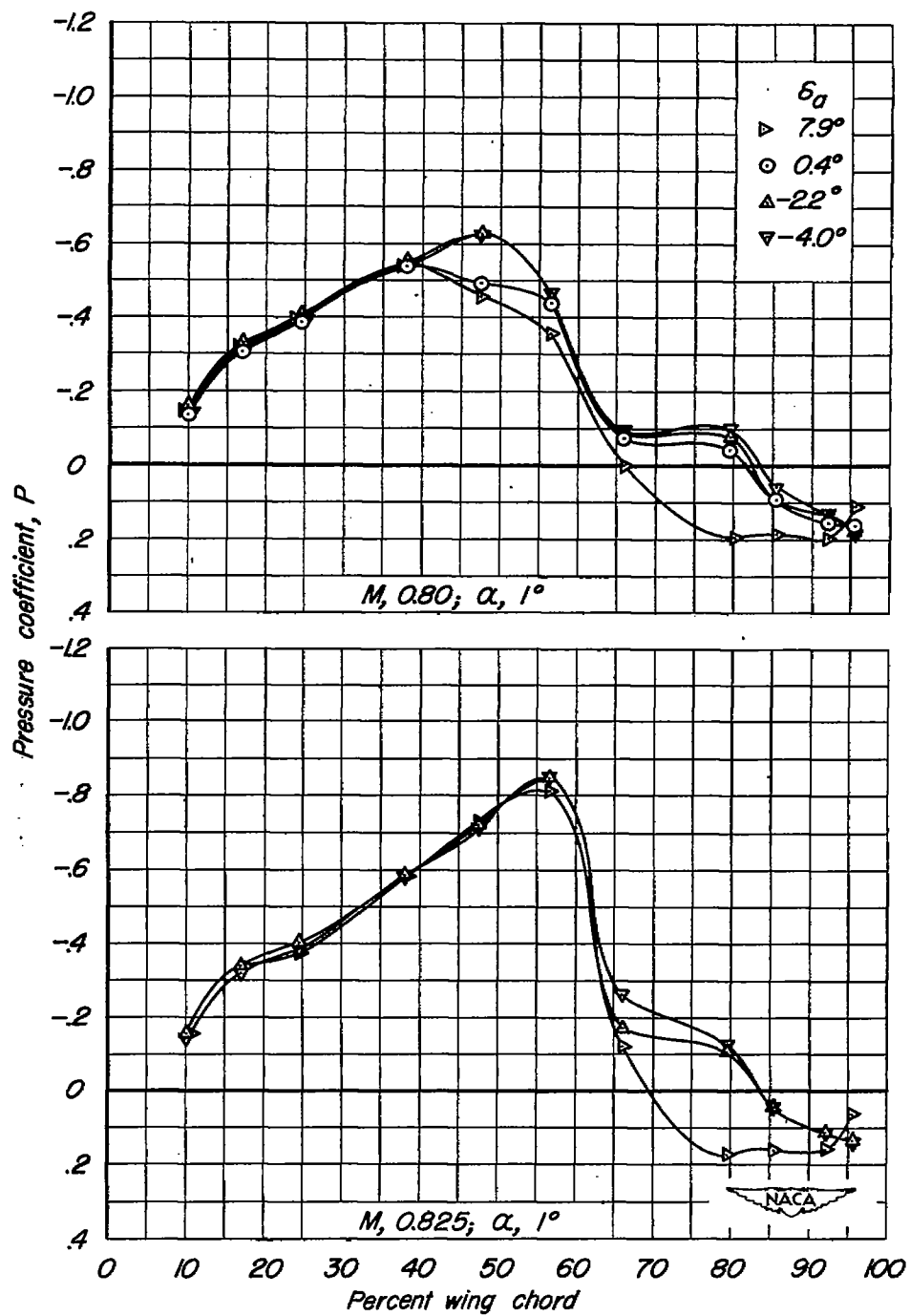


Figure 10.— Static lower-surface pressure coefficient for several aileron angles.

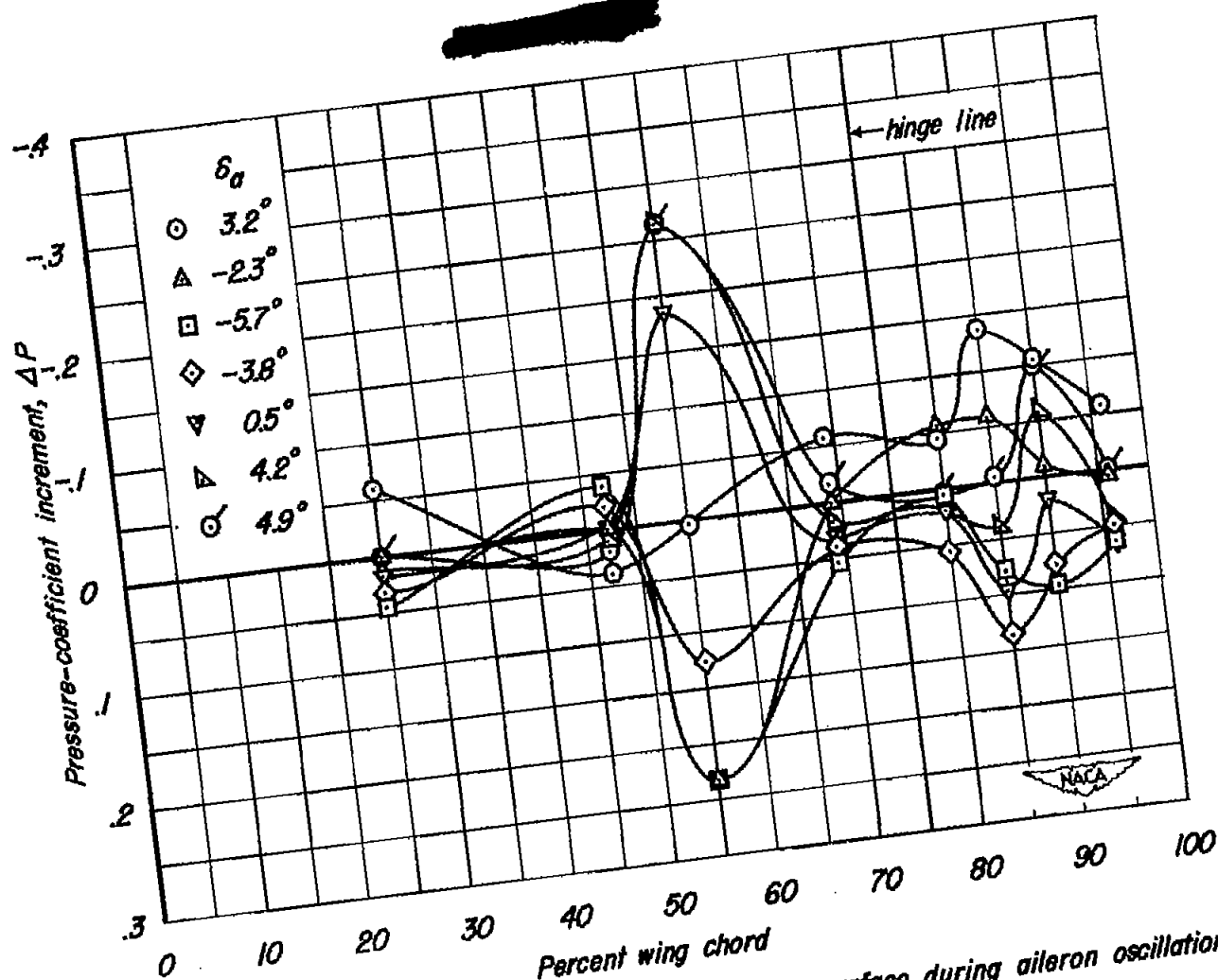


Figure 11. — Chordwise variation of pressure on the upper surface during aileron oscillations.

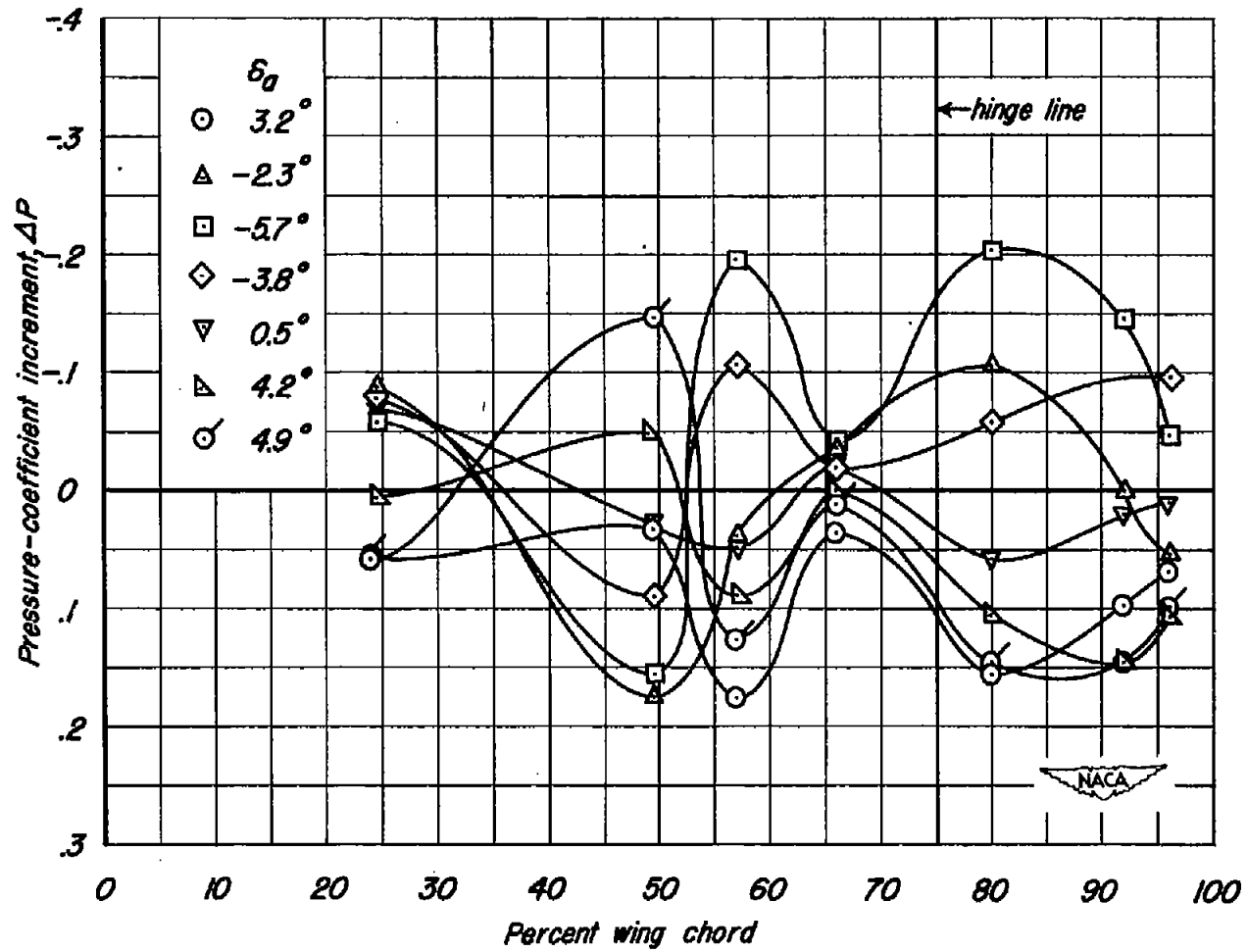


Figure 12 - Chordwise variation of pressure on the lower surface during aileron oscillations.

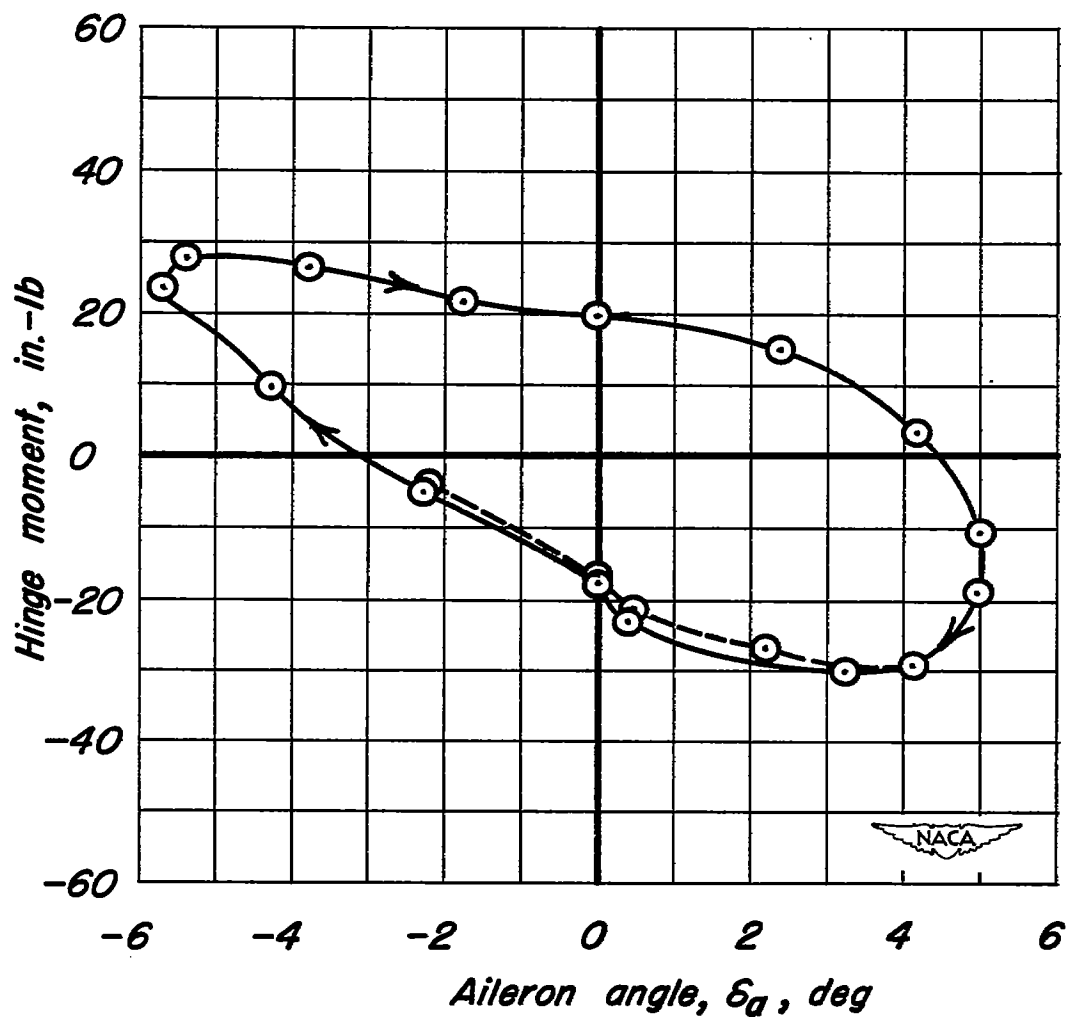


Figure 13.—Instantaneous hinge moments on the upper surface as a function of aileron angle for one inch of span.

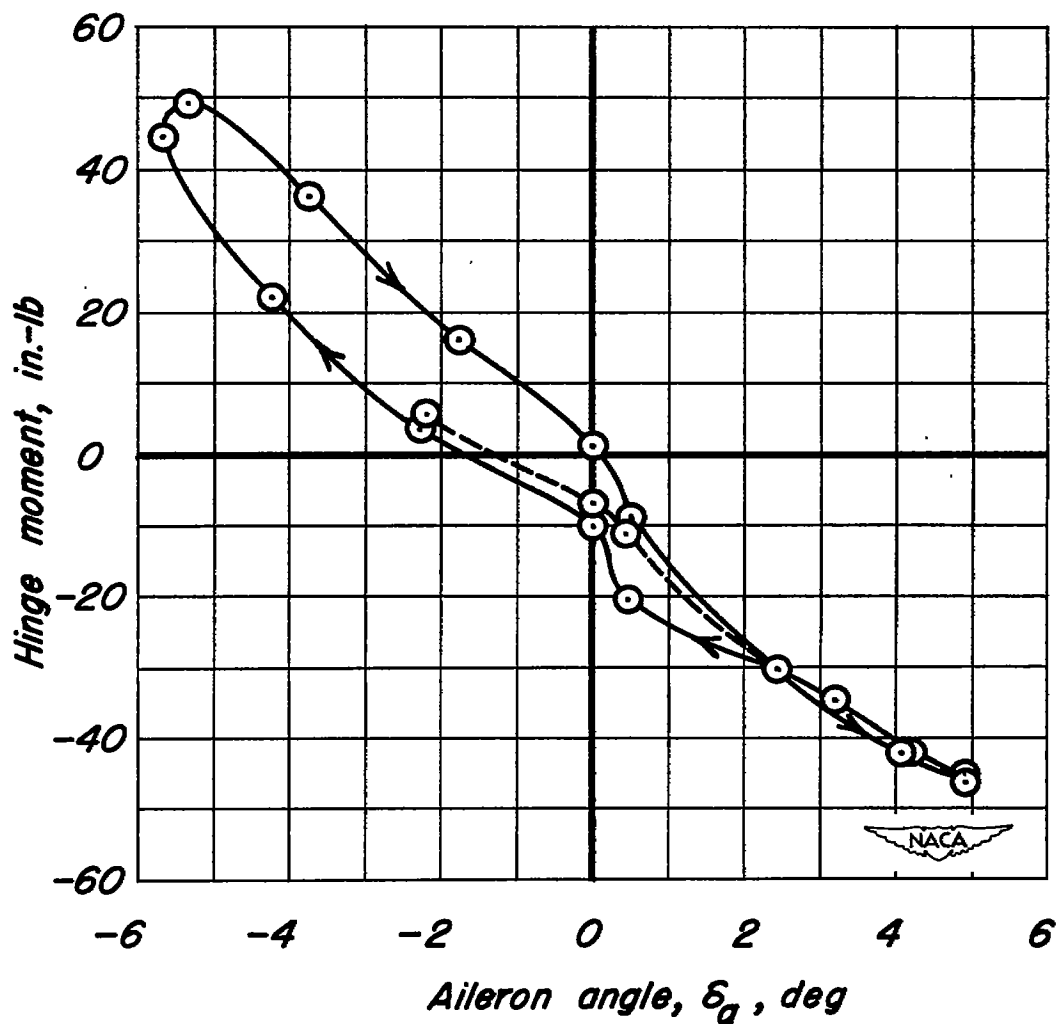


Figure 14.—Instantaneous hinge moments on the lower surface as a function of aileron angle for one inch of span.

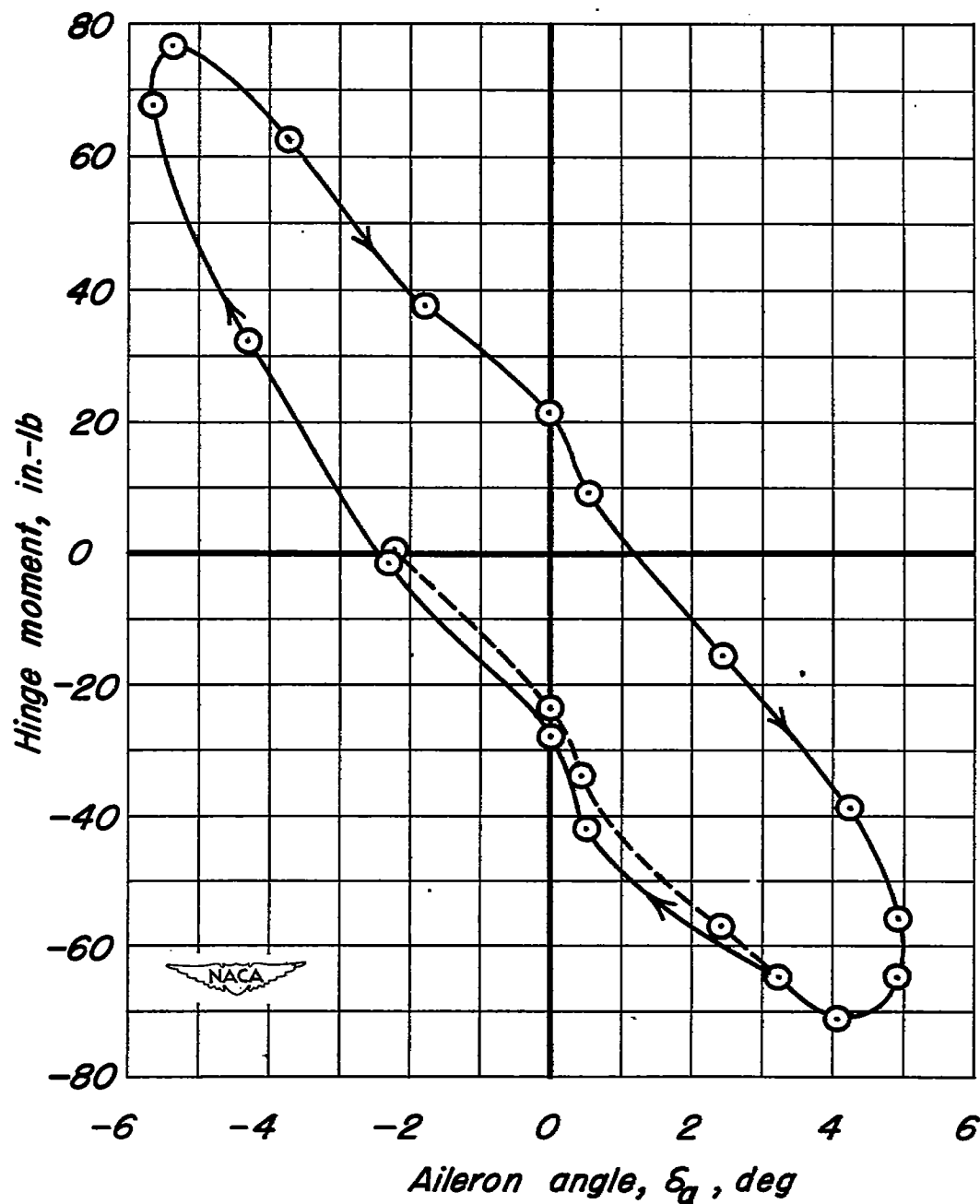


Figure 15.—Total instantaneous hinge moments for one inch of span as a function of aileron angle.

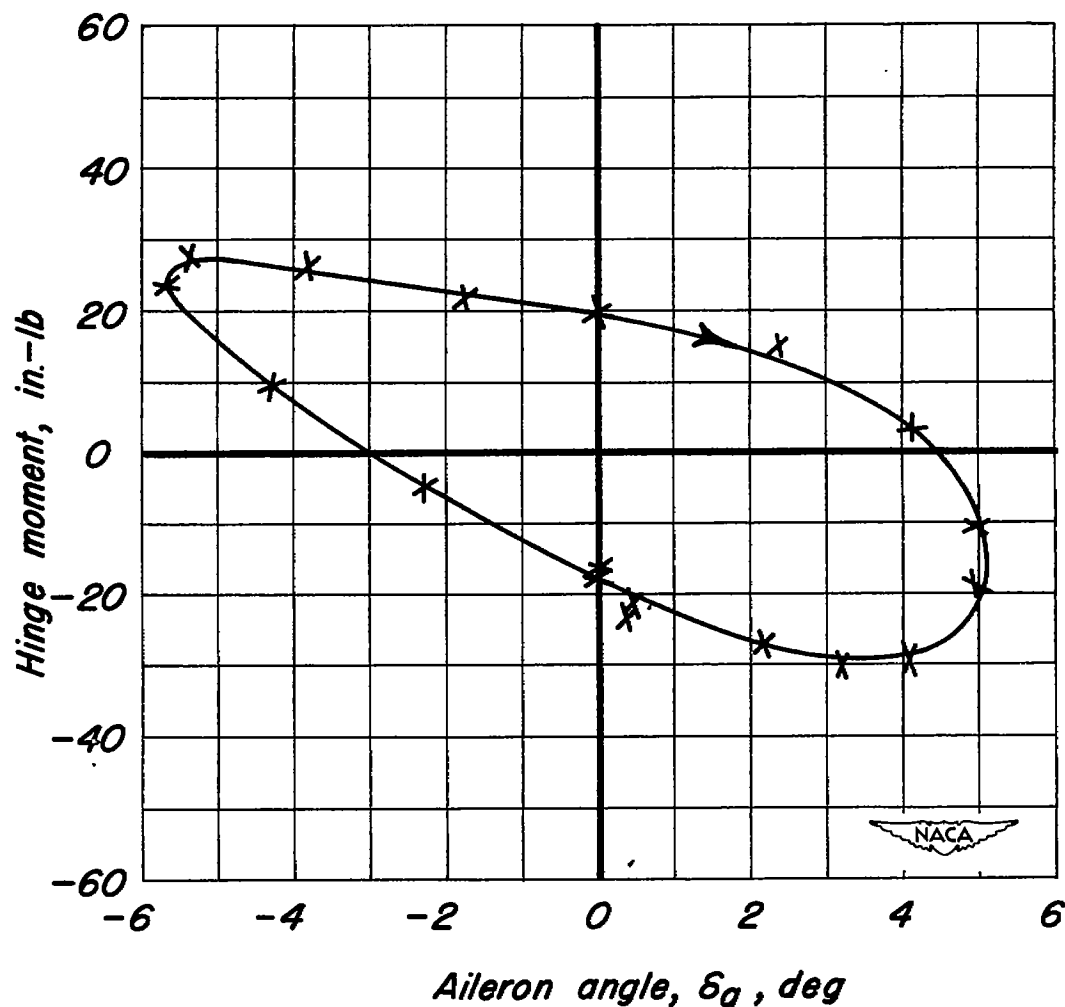


Figure 16.—Upper-surface hinge moments, for one inch of span, as a function of aileron angle computed from the first and second harmonics of the experimental data with the test points shown.

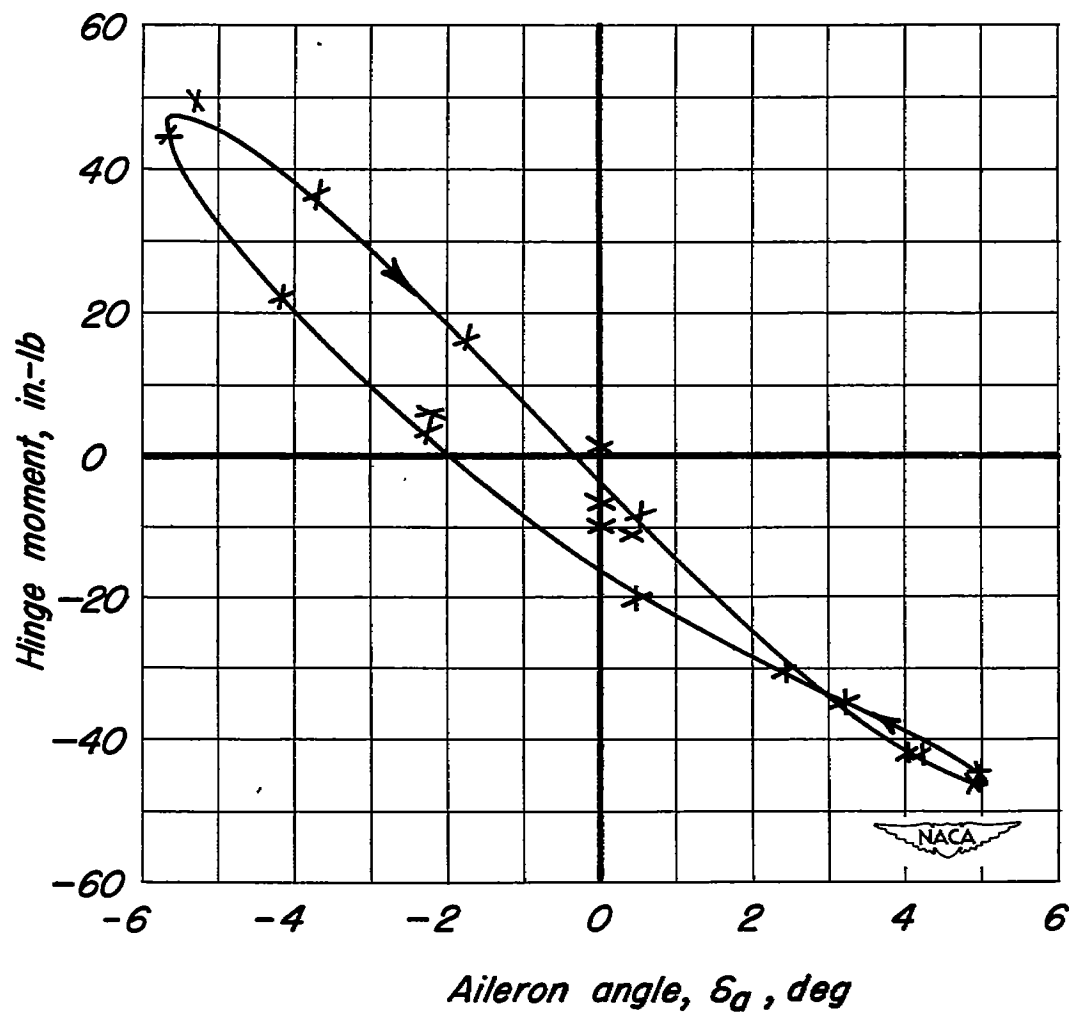


Figure 17.—Lower-surface hinge moments, for one inch of span, as a function of aileron angle computed from the first and second harmonics of the experimental data with the test points shown.

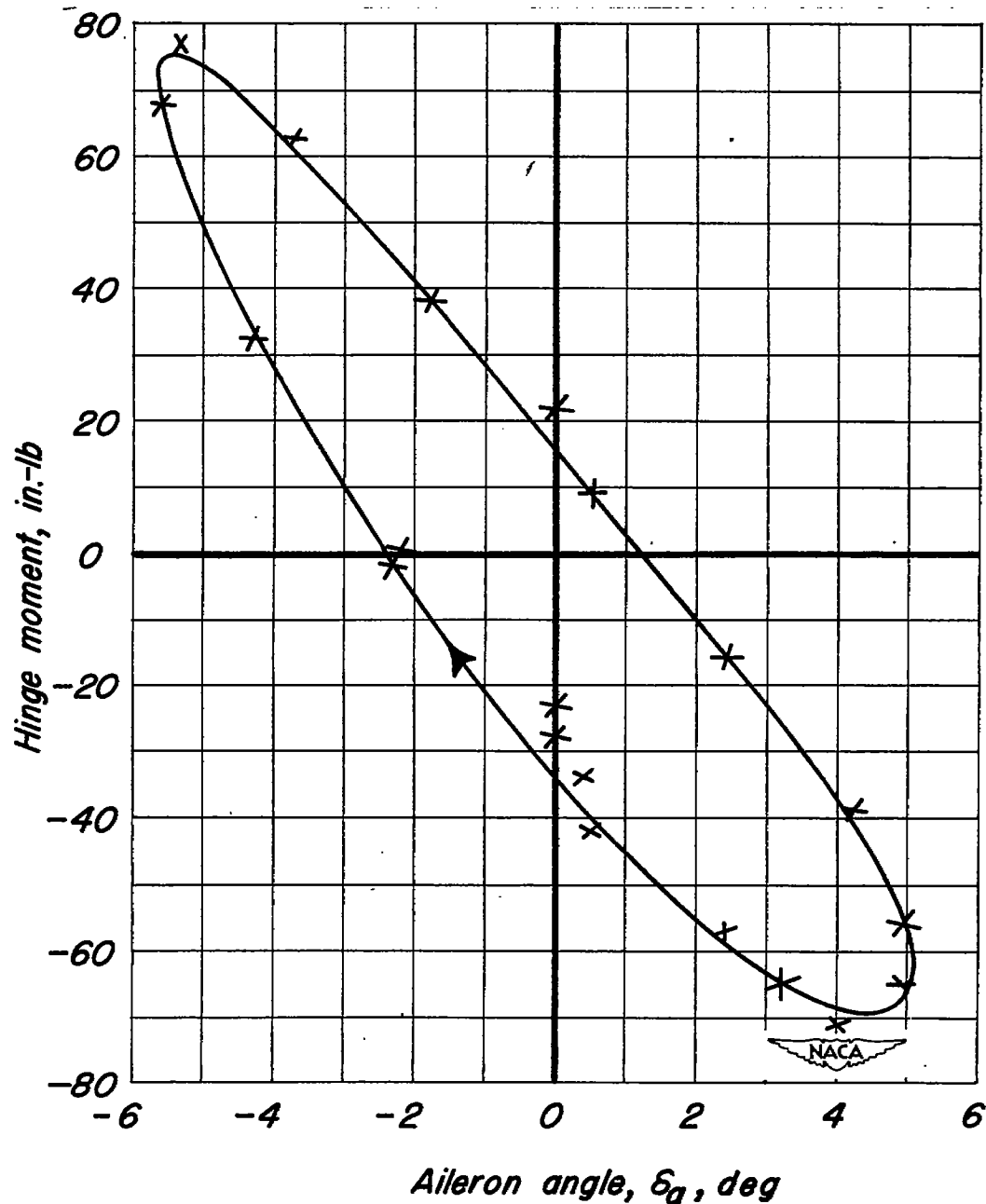


Figure 18.—Total hinge moments, for one inch of span, as a function of aileron angle computed from the first and second harmonics of the experimental data with the test points shown.

$$\delta_a = -4.65 \sin \omega t + 2.67 \cos \omega t$$

$$H = 45.13 \sin \omega t - 54.25 \cos \omega t$$

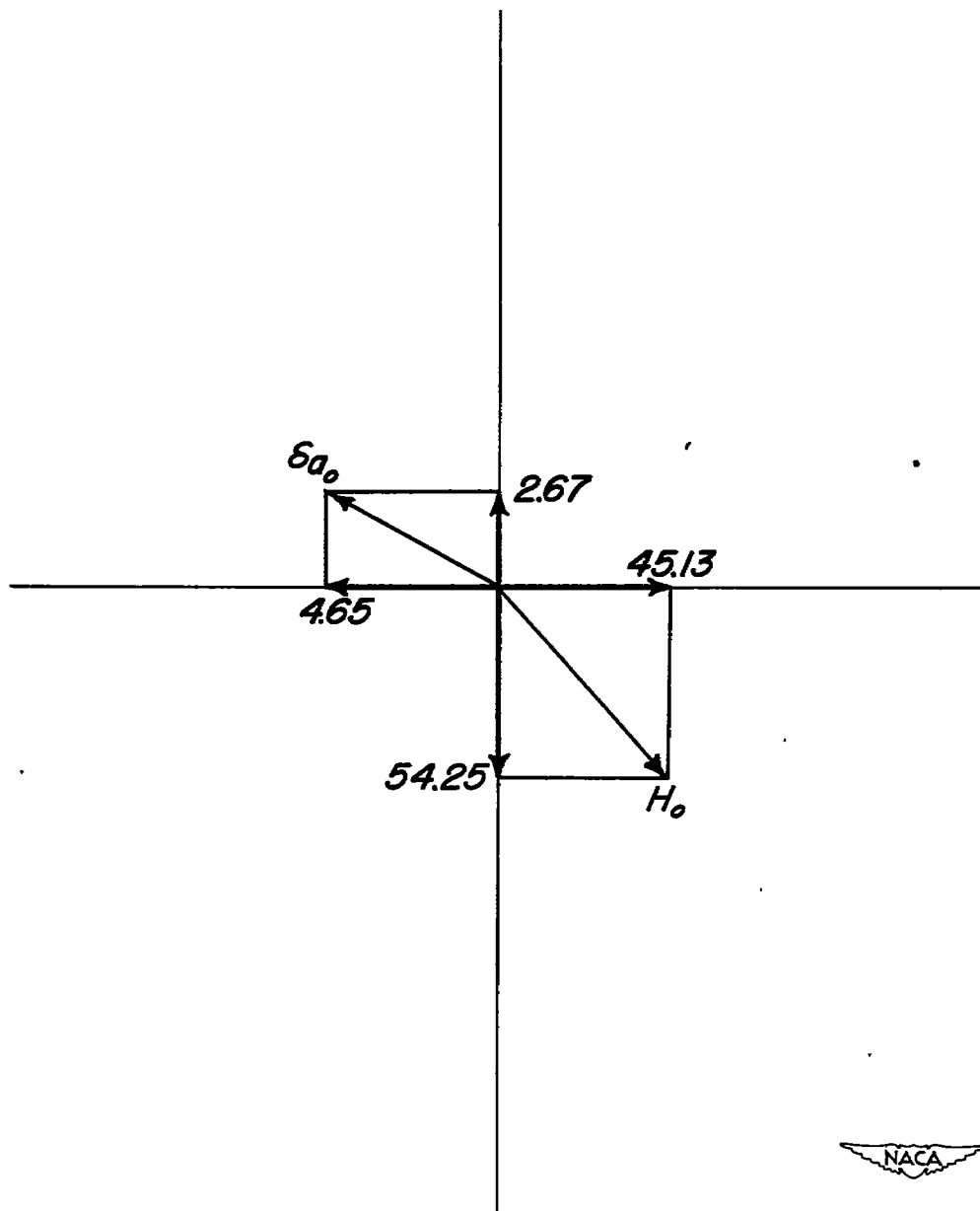


Figure 19.—Vector representation of the fundamentals of periodic aileron angle and aileron hinge moment obtained from harmonic analysis of experimental data. $\omega t, 0^\circ$.

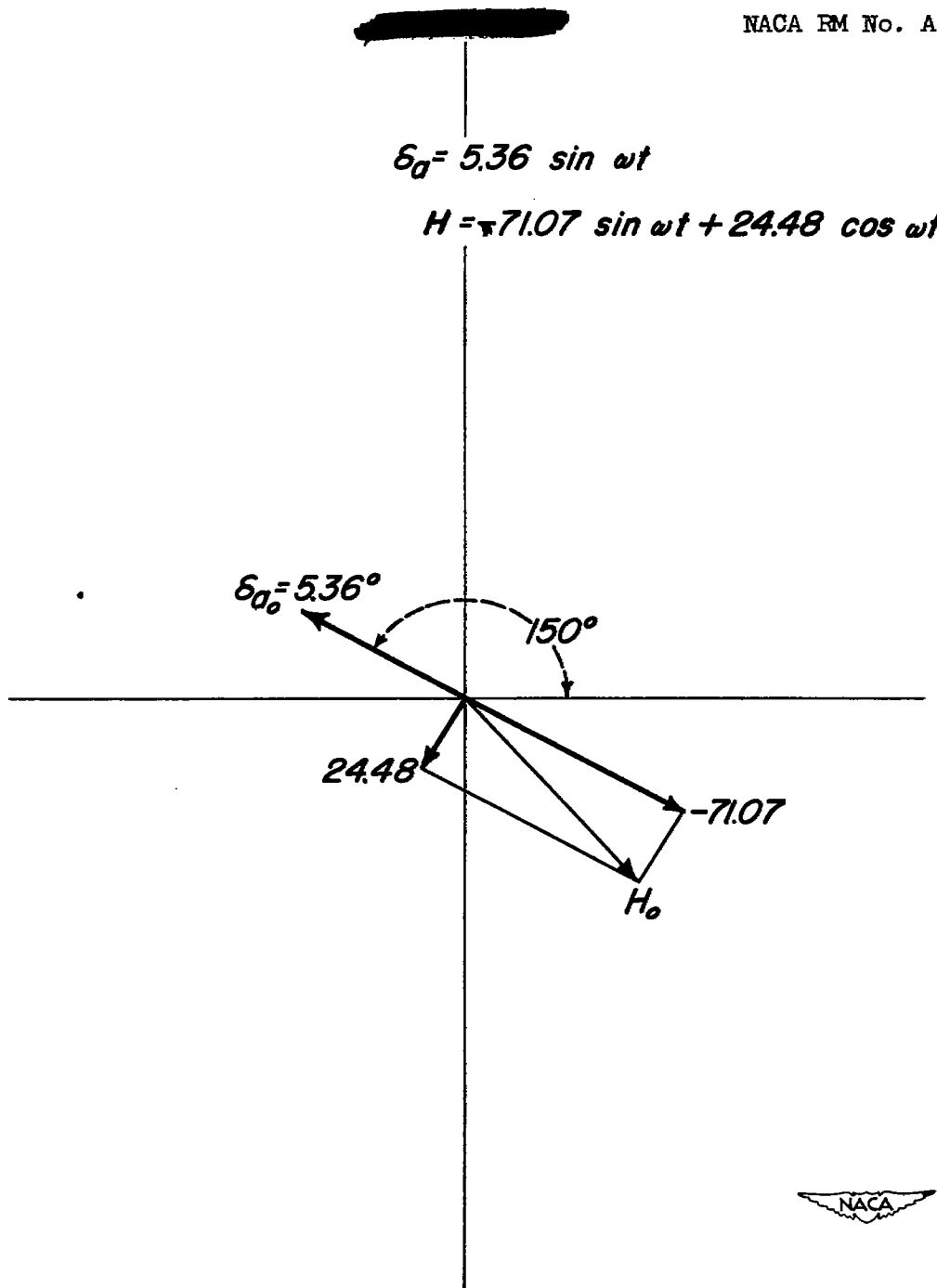


Figure 20.—Vector representation of the aileron and hinge-moment fundamentals with the hinge-moment vector resolved into components 90° and 180° out of phase with the resultant aileron vector. ωt , 150° .

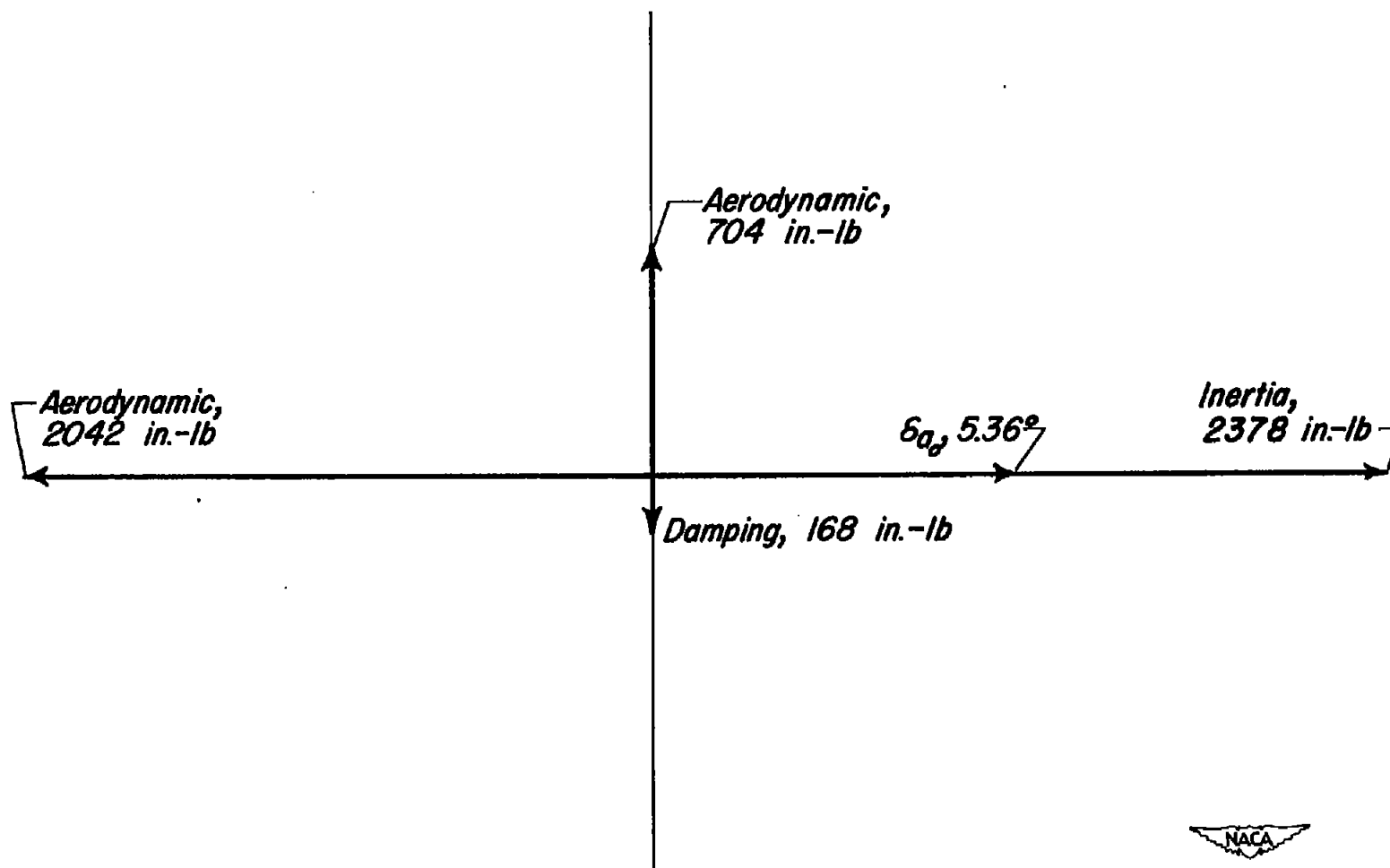


Figure 21.—Vector comparison of aerodynamic and mechanical hinge moments. $\omega t, 0^\circ$.

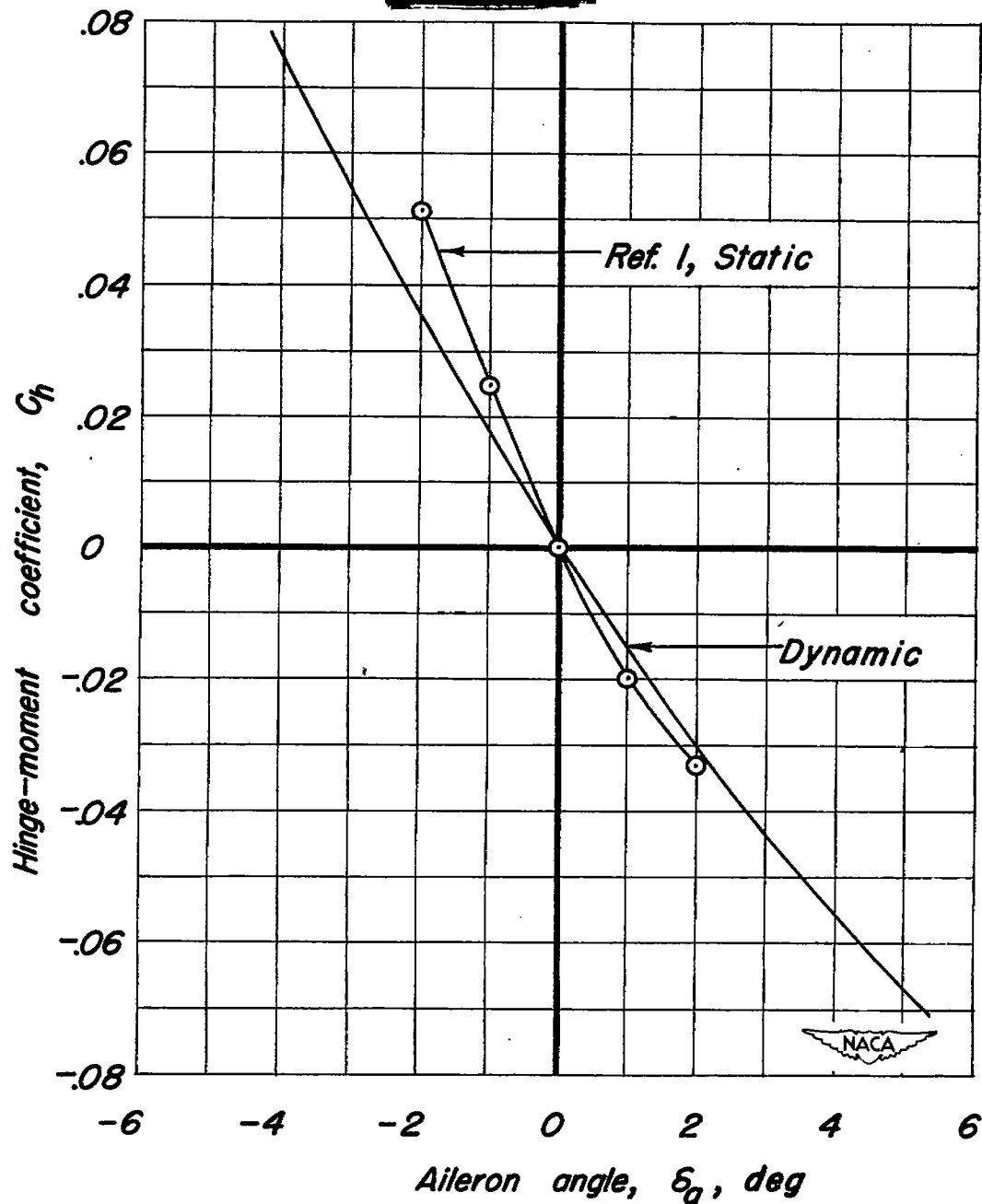
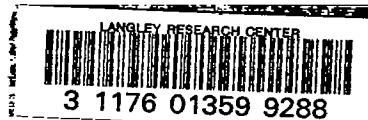


Figure 22.- Comparison of the experimental static hinge moment with the equivalent static hinge moment obtained from dynamic pressure-cell data.



DO NOT REMOVE SLIP FROM MATERIAL

Delete your name from this slip when returning material to the library.

NAME	DATE	MS
J. H. Hill	10/30/92	264